Desalination and Water Treatment
www.deswater.com
doi: 10.1080/19443994.2014.988653

57 (2016) 4162–4173
February

Taylor & Francis
Taylor & Francis Group

Preparation and characterization of chitosan/halloysite magnetic microspheres and their application for removal of tetracycline from an aqueous solution

Wei Ma[a,b], Jiangdong Dai[a], Xiaohui Dai[a], Zulin Da[a], Yongsheng Yan[a,*]

[a]*Department of Chemical Engineering, School of Chemistry and Chemical Engineering, Jiangsu University, 212013 Zhenjiang, P.R. China, Tel. +86 511 88789636; Fax: +86 511 88781119; emails: maweihenan@126.com (W. Ma), ujs2013djd@163.com (J. Dai), daixiaohui@ujs.edu.cn (X. Dai), 253258398@qq.com (Z. Da), mawei21899@163.com (Y. Yan)*
[b]*School of Chemistry and Chemical Engineering, Pingdingshan University, 467099 Pingdingshan, P.R. China*

Received 13 March 2014; Accepted 7 November 2014

ABSTRACT

In the work, magnetically separable adsorbent, named chitosan (CTS)/halloysite nanotubes (HNT)HNT-Fe_3O_4 microspheres are prepared by emulsion cross-linking method and characterized by Fourier transform infrared spectroscopic analysis, vibrating sample magnetometer, X-ray powder diffraction, scanning electron microscope, and transmission electron microscopy. The microspheres are applied as adsorbents for the removal of tetracycline (TC) from aqueous solution. The effects of the initial concentration of TCs solution (C_0), temperature, initial pH value (pH_0) of TC solution, and the adsorption dose on the adsorption capacity of the microspheres are investigated. The optimum pH value for TC adsorption is found at pH 5.0, and the adsorption capacity increased with the increase in adsorption temperature. The adsorption kinetics is better described by the pseudo-second-order equation, and their adsorption isotherms are better fitted to the Langmuir equation. CTS/HNT-Fe_3O_4 microspheres could be easily separated from the aqueous solution in a magnetic field. The adsorption–desorption experiments implied that CTS/HNT-Fe_3O_4 microspheres can be used as promising adsorbents for the removal of TC from wastewater HNT.

Keywords: Chitosan; Halloysite; Magnetic microspheres; Adsorption; TC

1. Introduction

In the past decades, antibiotics have been widely used for treating humans and animals, and as growth promoters in livestock and aquaculture operations [1]. Tetracycline (TC, $C_{22}H_{24}N_2O_8$) exhibits broad-spectrum antimicrobial activity against a variety of bacteria and it is the second most widely used antibiotics in the world [2]. However, these pharmaceuticals are very difficult to be metabolized completely and their residues left in the environment can induce the development of antibiotic-resistant pathogens and pose adverse health effects to humans [3–5]. Therefore, it is of great necessity to develop efficient and inexpensive treatment methods for the removal of such compounds from the environment [6].

Various techniques such as ozonation [7], photo-Fenton process [8], photoelectrocatalytic degradation [9,10], and adsorption [11–16] have been employed for the removal of tetracycline from water. Among these

*Corresponding author.

methods, adsorption is considered as one of the most effective methods due to its simple operation, high treatment efficiency, and low value [17]. Biomass adsorbents have caused a growing concern in view of sustainable development and environmental protection, and biomass adsorbents have advantages with extensive sources, low price, renewable property, and biodegradable property. Chitosan (CTS), one of the high performance natural polysaccharide material composed of randomly distributed β-(1-4)-linked D-glucosamine and N-acetyl-D-glucosamine [18], is a biodegradable and biocompatible polymer which can be obtained by alkaline deacetylation of chitin. The chitin is the main component of the exoskeleton of crustaceans and the second most abundant biopolymer in nature. CTS can remove various contaminants from wastewater because of its hydroxyl and amino groups. However, drawbacks such as poor mechanical strength, low specific gravity, easy agglomeration or gel formation, and insufficient solubility in dilute acids largely limit its widespread applications for environmental pollutant removal [19,20]. Mechanical strength, chemical stability, hydrophilicity, and biocompatibility of CTS can be improved by modification. To improve the chemical stability, many cross-linking agents such as glutaraldehyde, glyoxal, and epichlorohydrin were used [21,22].

Incorporation of nanosized inorganic materials such as hydroxyapatite, nanoclay, carbon nanotubes, titanium dioxide, and graphene into CTS can improve the mechanical properties of CTS [23]. Halloysite nanotube (HNT) is an environmentally friendly and abundant in nature as a raw material that can be mined from the corresponding deposit as a raw mineral [24]. Since HNT possess some excellent characteristics, such as large surface area, good mechanical and thermal properties, large pore volume, and adequate hydroxyl groups [25], HNT have been used as the removal of environmental pollutant [26], and HNT can improve adsorption and oil entrapment capacity [27,28]. HNT are one-dimensional nanoparticles with hollow nanotubular structure which can be employed for preparing the CTS microspheres. These HNT nanotubes showed the potential to improve the mechanical properties and thermal stability of HNT of the CTS microspheres [29]. Recently, magnetic separation technology (MST) is gaining growing attention [30,31]. With the aid of magnetic force, magnetic microspheres can be separated from the water efficiently regardless of their size. Magnetite (Fe_3O_4) has been widely used as magnetic material because of its merits of high dispersion stability, excellent biocompatibility, high magnetic susceptibility, and chemical stability [32]. The combination of MST and adsorption process has been widely developed [33]. However, the preparation of CTS/HNT-Fe_3O_4 microspheres and the removal of the TC by the adsorbent have never been reported.

In this study, firstly, iron oxide nanoparticles were synthesized on the surface of HNT to prepare the magnetic HNT-Fe_3O_4; secondly, CTS/HNT-Fe_3O_4 microspheres were prepared by emulsion cross-linking method. The effects of various experimental conditions, such as different dosage of CTS/HNT-Fe_3O_4 microspheres, initial pH value, initial concentration, and adsorption temperature, were investigated. In order to study the mechanism of the adsorption, the collected experiment data was fitted to kinetic and equilibrium models.

2. Experiments

2.1. Materials

The HNT were obtained from Henan province, China; TC was purchased from Shanghai Shunbo Biological Engineering Co., Ltd.; iron (III) chloride hexahydrate ($FeCl_3{\cdot}6H_2O$), iron (II) chloride tetrahydrate ($FeCl_2{\cdot}4H_2O$), glutaraldehyde, ammonia water, petroleum ether, isopropanol, ethanol, CTS (80.0–95.0% acetylation degree), liquid paraffin, and span-80 were obtained from Sinopharm Chemical Reagent Co., Ltd. (Shanghai, China). All are analytical grade reagents. Deionized ultrapure water was purified with a Purelab ultra (Organo, Tokyo, Japan).

Stock solutions (1,000 mg L^{-1}) were prepared by dissolving TC in deionized water. One molar solutions of HCl and NaOH were used for pH adjustments.

2.2. Preparation of HNT-Fe_3O_4 and CTS/HNT-Fe_3O_4 microspheres

2.2.1. Preparation of HNT-Fe_3O_4

HNT-Fe_3O_4 material was prepared via improved co-precipitation technique [34,35]. The HNT-Fe_3O_4 were prepared from a suspension of 1-g HNT in a 180-mL solution of 4.72-g $FeCl_3{\cdot}6H_2O$ and 2.1-g $FeCl_2{\cdot}4H_2O$ at 60°C under N_2, $NH_3{\cdot}H_2O$ solution was added dropwise to prepare iron oxides. The pH of the final mixtures was controlled in the range of 9–11. The mixtures were aged at 70°C for 4 h and then washed three times with distilled water. The obtained compounds were dried in a vacuum oven, at 60°C.

2.2.2. Preparati on of CTS/HNT-Fe_3O_4 microspheres

In 25-mL 2% (v/v) acetic acid solution, 0.5 g CTS was dissolved. Then, 0.25-g HNT-Fe_3O_4 was dispersed

into the CTS solution under mechanical stirring for 2 h at 1,500 rpm, 100-mL paraffin and 4-mL emulsifier (Span-80) were poured into the prepared CTS dispersion solution under mechanical stirring at 40℃. After stirring for 1 h, 2-mL glutaraldehyde (25%, v/v) was slowly dropped into the reaction system and stirred in a water bath at 60℃ for another 1 h, and then, the prepared product was centrifuged and washed with petroleum ether, ethanol, and distilled water for three times, respectively. Finally, the product was dried in a vacuum oven at 60℃.

2.3. Characterization

Fourier transform infrared (FT-IR) spectra were recorded on a Nicolet Nexus 470 FT-IR (America thermo-electricity Company) with 2 cm^{-1} resolution in the range 400–4,000 cm^{-1}, using KBr pellets. UV–vis absorption spectra were obtained using a Specord 2450 spectrometer (Shimazu, Japan). The measurements of magnetic particles were carried out using a vibrating sample magnetometer (VSM, HH-15, China) under a magnetic field up to 10 kOe. X-ray diffraction (XRD) technique was used to characterize the crystal structure of prepared microspheres. In this work, XRD patterns were obtained with a D/max-RA X-ray diffractometer (Rigaku, Japan) equipped with Ni-filtrated Cu Ka radiation (40 kV, 200 mA). The 2θ scanning angle range was 10–70˚ with a step of 0.02˚/0.2 s. The SEM images were examined with S-4800 scanning electron microscopy (HITACHI, Japan). TEM micrographs were taken with a JEOL-JEM-2010 (JEOL, Japan) operated at 200 kV.

2.4. TC removal experiments

Adsorption experiments were carried out using CTS/HNT-Fe_3O_4 microspheres as adsorbent on a temperature-controlled incubator shaker set at 100 rpm maintained at 25℃ for 80 min. A known amount of adsorbent was thoroughly mixed with 20 mL of respective TC solutions, whose concentration and pH_0 were previously known, pH of the reaction mixture was initially adjusted using either hydrochloric acid or sodium hydroxide (1 M). After the adsorption, the CTS/HNT-Fe_3O_4 microspheres were separated rapidly from the solutions using a magnet, supernatants were analyzed for TC concentration using UV–vis spectrophotometer at 275.6 nm. The adsorption of TC on CTS/HNT-Fe_3O_4 microspheres was performed for different intervals (0–80 min), initial pH (1.0–7.0), initial TC concentrations (20–180 mg L^{-1}), adsorbent dose (10.0–50.0 mg), and adsorption temperature (298, 308 K) in 20-mL aqueous solution. The equilibrium adsorption amounts of TC were calculated according to the following equation:

$$Q_e = \frac{(C_0 - C_e)V}{m} \quad (1)$$

where Q_e (mg g^{-1}) is the amount of TC adsorbed at equilibrium, C_0 and C_e (mg L^{-1}) are the concentrations of TC at initial and equilibrium, respectively. V is the volume of TC solution, and m is the weight of the CTS/HNT-Fe_3O_4 microspheres.

Studies on the adsorption kinetics were identical with equilibrium tests, the initial concentration was set as 100 mg L^{-1}, and the adsorbents were separated at predetermined time intervals. The amount of TC adsorbed (Q_t, mg g^{-1}) was calculated according to the following equation:

$$Q_t = \frac{(C_0 - C_t)V}{m} \quad (2)$$

where C_t (mg L^{-1}) is the concentration of TC solution at any time t.

3. Results and discussion

3.1. FT-IR

Fig. 1 exhibits the FT-IR spectra of HNT-Fe_3O_4 and CTS/HNT-Fe_3O_4 microspheres. The double peaks at 3,692 and 3,620 cm^{-1}, respectively, were due to the stretching vibrations of hydroxyl groups at the surface

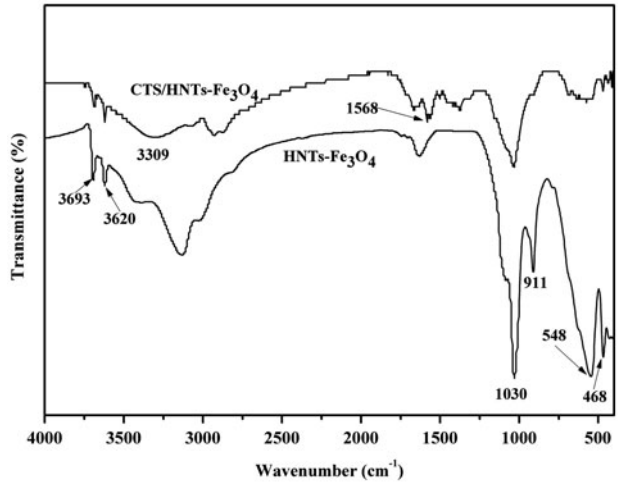

Fig. 1. The FT-IR spectra of HNT-Fe_3O_4 and CTS/HNTs-Fe_3O_4 microspheres.

of CTS/HNT-Fe_3O_4 microspheres and HNT [36]. The peak at 1,030 cm^{-1} was assigned to Si–O groups in HNT. The deformation of Si–O–Si, deformation of Al–O–Si, and O–H deformation of inner hydroxyl groups exhibited the peaks at 468, 543, and 911 cm^{-1}, respectively [37]. HNTHNTAnd, the band of Al–O–Si of HNT at 543 cm^{-1} and characteristic peak of the Fe_3O_4, at around 580 cm^{-1} [38] could be overlapped in CTS/HNT-Fe_3O_4 microspheres and HNT-Fe_3O_4. All the above characteristic peaks of HNT and Fe_3O_4 appeared in FT-IR spectra of HNT-Fe_3O_4 and CTS/HNT-Fe_3O_4 microspheres, it demonstrated that HNT and Fe_3O_4 exist in the HNT-Fe_3O_4 and CTS/HNT-Fe_3O_4 microspheres [35]. In the FT-IR spectrum of CTS [39,40], there are two characteristic peaks at 1,545 and 1,405 cm^{-1}, which correspond to the deformation vibration of the protonated amine group ($-NH_3^+$) and hydroxyl group, respectively. The two peaks for the CTS/HNT-Fe_3O_4 microspheres slightly shift to higher frequencies (i.e. the absorbance band of NH_2 vibration moves from 1,545 to 1,568 cm^{-1} for the microspheresHNT) due to the electrostatic interactions and H-bonding interaction between HNT and CTS. The broad peaks around 3,208 cm^{-1}, which are attributed to the overlapped N–H band and O–H band vibration of the CTS [41], also moves to higher frequencies (around 3,309 cm^{-1}) in the microspheres. These changes in FT-IR spectrum show the interactions between HNT and CTS via the electrostatic interaction and hydrogen bonding.

3.2. SEM and particle distribution curve

As shown in Fig. 2, the morphologies of HNT-Fe_3O_4 and CTS/HNT-Fe_3O_4 microspheres were obtained by scanning electron microscope (SEM). In Fig. 2(A) and (B), HNT-Fe_3O_4 was attached with clusters of Fe_3O_4. HNT. The attachment could be related to the structures of HNT, such as the large surface area, large pore volume, and adequate hydroxyl groups [25]. Fig. 2(C) and (D) presents SEM micrographs of CTS/HNT-Fe_3O_4 microspheres. The surface of microsphere is uneven, it can be seen that parts of the HNT-Fe_3O_4 are likely to absorb on the surface of the CTS/HNT-Fe_3O_4 microspheres. However, it is difficult to accurately calculate the amount of HNT-Fe_3O_4 on the surface and inside the microspheres. Fig. 3 exhibits SEM particle distribution curve of the CTS/HNT-Fe_3O_4 microspheres, it can be seen that particle size of the microspheres is mainly distributed between 4 and 8 μm, the average particle size of the microspheres was 5.7 μm. It shows that the prepared microspheres have consistent size.

3.3. TEM

Fig. 4 presents TEM micrographs of HNT and HNT-Fe_3O_4. HNT (Fig. 4(A)) showed the nanotubes with the smooth surface, open ends, and hollow cavity of about 20 nm in diameter [35]. In Fig. 4(B–D), clusters of Fe_3O_4 gathered at the surface of HNT-Fe_3O_4. And, few Fe_3O_4 nanoparticles were found to adhere on the wall of the hollow cavities of HNT. HNT have large surface area, large pore volume, and adequate hydroxyl groups, which can be used as adsorbent for TC. It can be seen that the obtained HNT and HNT-Fe_3O_4 in this work have better dispersion when compared to previous work by TEM micrographs [35].

3.4. XRD

The power XRD patterns of the HNT-Fe_3O_4 and CTS/HNT-Fe_3O_4 microspheres are shown in Fig. 5. The powder XRD patterns of HNT-Fe_3O_4 and CTS/HNT-Fe_3O_4 microspheres displayed distinct peaks at 2θ values of about 30.09, 35.44, 43.08, 53.44, 56.97, and 62.55, as marked in Fig. 5. These peak positions and relative peak intensities corresponded to the characteristic peaks of Fe_3O_4 [42]. It illustrated therefore that HNT-Fe_3O_4 were successfully introduced to the HNT-Fe_3O_4 and CTS/HNT-Fe_3O_4 microspheres. In Fig. 5, the peaks for HNT are not detected, This is mainly because, content of HNT is lower and characteristic peaks of HNT have been diluted in the HNT-Fe_3O_4 and CTS/HNT-Fe_3O_4 microspheres.

3.5. Magnetic properties

Magnetization properties of CTS/HNT-Fe_3O_4 microspheres were studied by VSM, as shown in Fig. 6, the curves were symmetrical and passed through the origin with no hysteresis, suggesting that it is typical characteristic of super paramagnetic particles [43]. HNT Magnetization increased with an increase in the magnetic field. The saturation magnetization values of CTS/HNT-Fe_3O_4 microspheres was 6.80 emu g^{-1}, measured at 298 K, HNT. The obtained Ms value of CTS/HNT-Fe_3O_4 microspheres in this work was low when compared to the prepared HNT-Fe_3O_4 in previous works [35], where the Ms values of

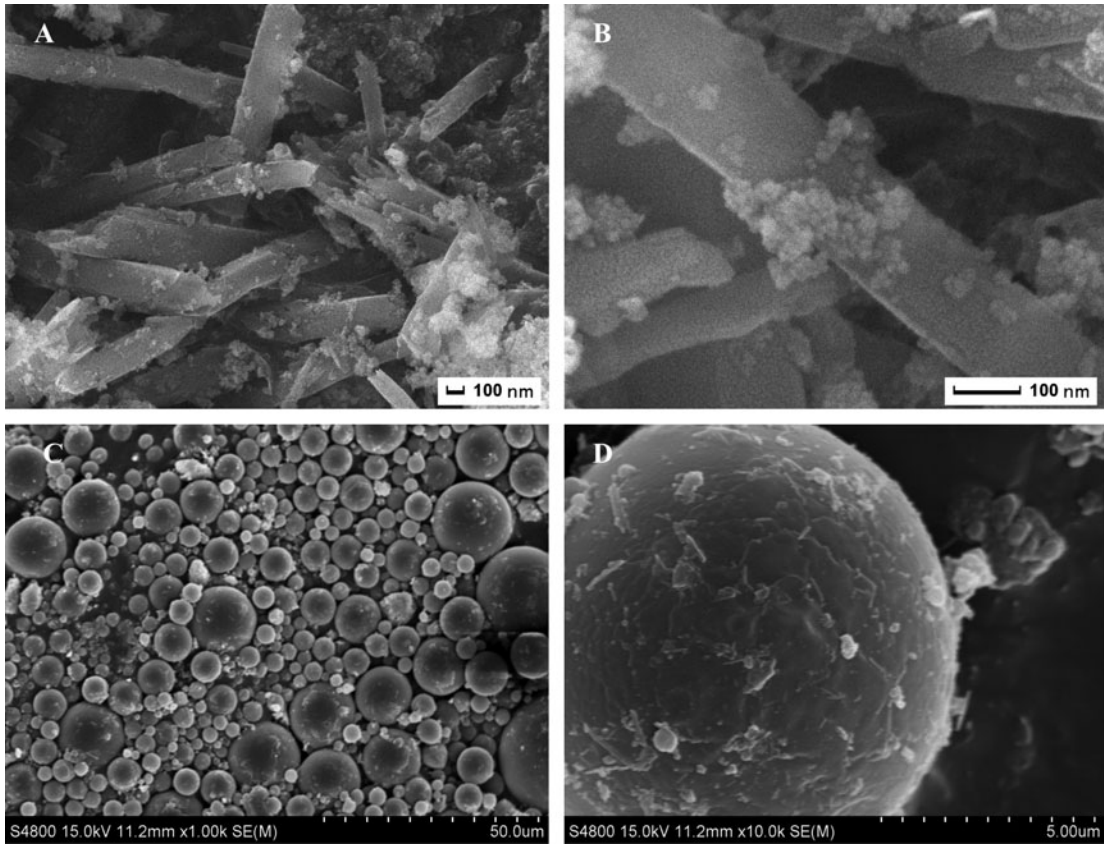

Fig. 2. The SEM images of HNT-Fe_3O_4 (A) and (B) and CTS/HNTs-Fe_3O_4 microspheres (C) and (D).

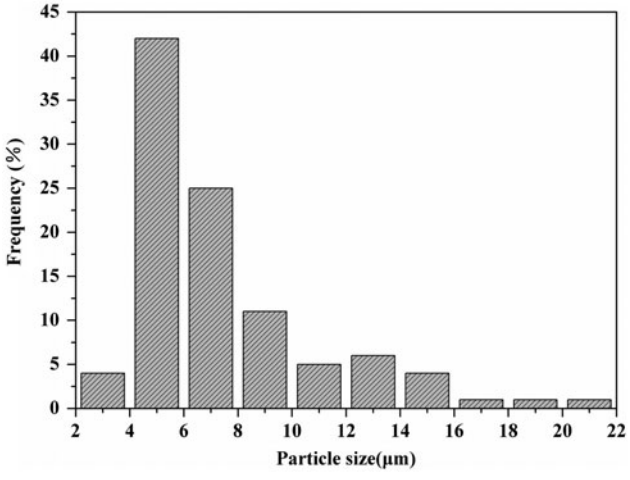

Fig. 3. The SEM particle distribution curve of CTS/HNTs-Fe_3O_4 microspheres.

HNT-Fe_3O_4 was 27.91 emu g^{-1}, CTS/HNT-Fe_3O_4 microspheres can still be separated from the water with the help of an external magnet.

3.6. Adsorption of the TC

3.6.1. Effect of adsorbent dose and initial concentration of TC on TC adsorption

The effect of adsorbent dose and initial concentration on the adsorption capacity of CTS/HNT-Fe_3O_4 microspheres are studied in Fig. 7. It is observed that the adsorption capacity of microspheres increased with an increase in the dose of CTS/HNT-Fe_3O_4 microspheres from 10.0 to 50.0 mg, at the same initial concentration. And, the adsorption capacity of microspheres increased with an increase in initial concentration at the same dose of CTS/HNT-Fe_3O_4 microspheres, this is because the higher initial concentration enhance the mass transfer driving force of the adsorbate in solid–liquid phase, and then, increase the adsorption capacity. In the dose of CTS/HNT-Fe_3O_4 microspheres increased from 20.0 to 50.0 mg at the initial concentration of 100 mg L^{-1}, the adsorption capacity of CTS/HNT-Fe_3O_4 microspheres only increased from 19.6 to 23 mg g^{-1}; it is due to the concentration gradient between adsorbent and adsorbate. The fact suggests that the economy absorbent dose is at 20.0 mg for the removal of TC in this system.

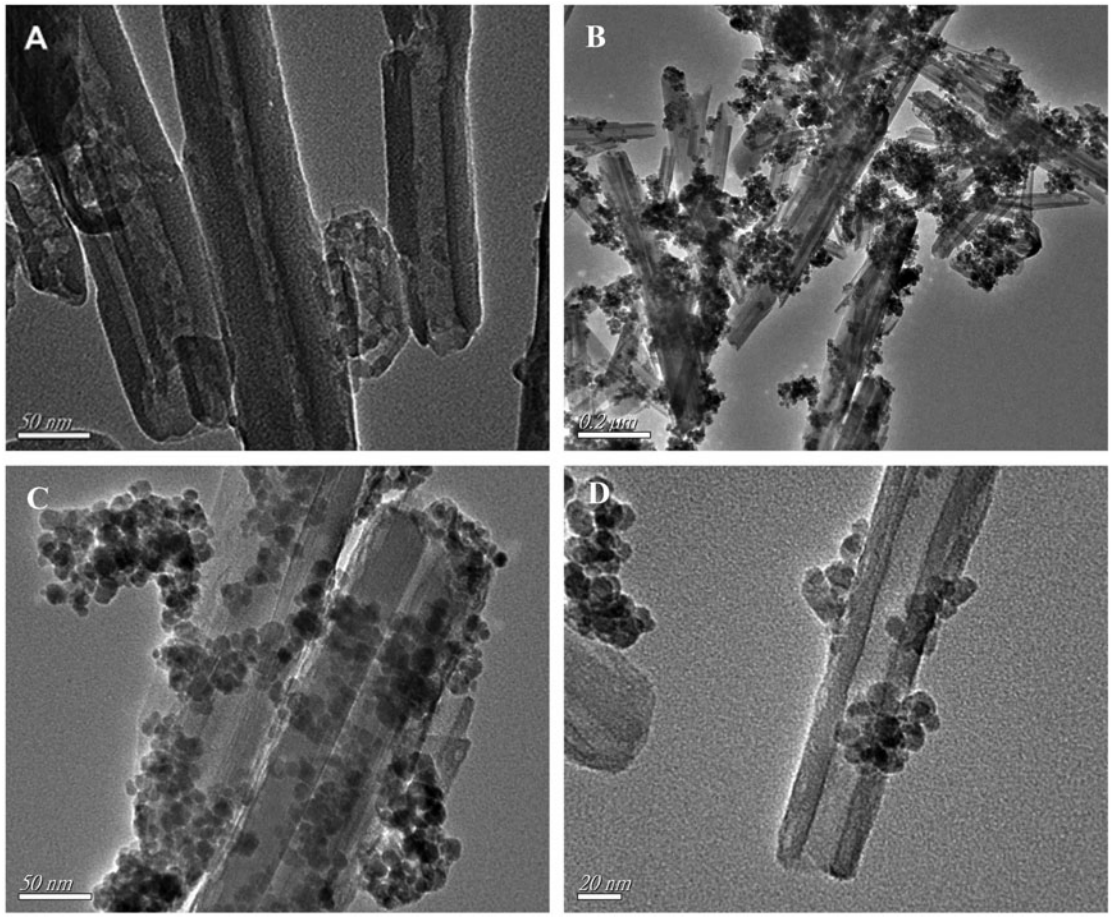

Fig. 4. The TEM images of HNT (A) and HNTs-Fe_3O_4 (B–D).

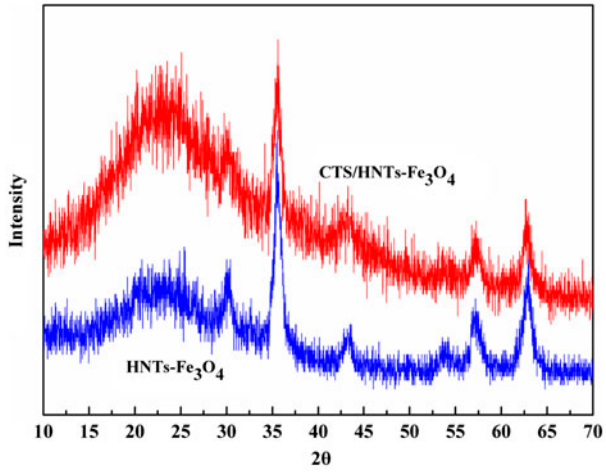

Fig. 5. Powder XRD patterns of HNT-Fe_3O_4 and CTS/HNTs-Fe_3O_4 microspheres.

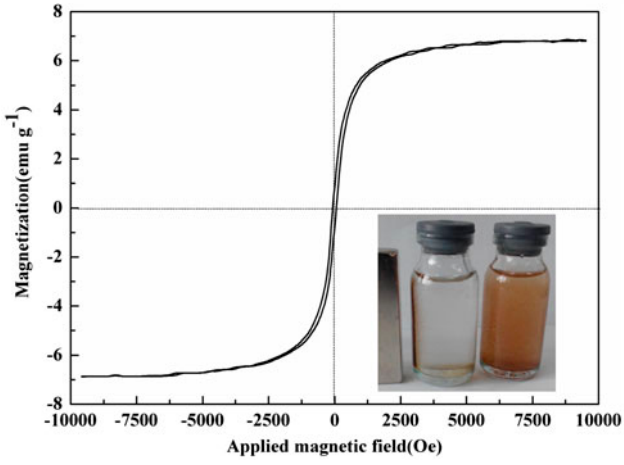

Fig. 6. Magnetic hysteresis loops of CTS/HNTs-Fe_3O_4 microspheres.

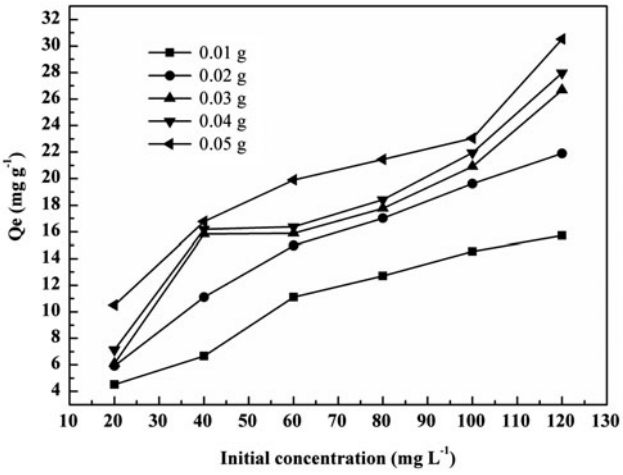

Fig. 7. Effect of adsorbent dose on and initial concentration of TCs on TCs adsorption (*V*: 20 mL; initial pH: 5.0; temperature: 298 K).

3.6.2. Effect of initial pH on TC adsorption

The effect of initial pH on the adsorption capacity of CTS/HNT-Fe_3O_4 microspheres are shown in Fig. 8. It was evident that the adsorption capacity was highly pH dependent and the maximum adsorption was found at pH 5.0. The initial pH of the TC solution was an important factor which influenced the adsorption process and the adsorption capacity, it is because pH of the solution can change the surface charge of the adsorbent, the degree of ionization of the adsorbate molecule, and extent of dissociation of functional groups on the active sites of the adsorbent [43]. The pKa_1, pKa_2, pKa_3 values of TC were 3.30, 7.70, and 9.70, respectively. When pH of the TC solution was between pKa_1 and pKa_2, TC was an amphoteric ion, CTS/HNT-Fe_3O_4 microspheres had the bigger adsorption capacity. When the solution pH was less than pKa_1 or greater than pKa_3, TC had positive and negative charges, the pKa of chitosan is around 6.20, below pH 5 almost 90% of active sites were protonated, the acting force of microspheres and TC decreased obviously. Therefore, the adsorption capacity of the microspheres decreased. Other experiments in this paper were carried out at pH 5.0.

3.6.3. Effect of initial concentration of TC and contact time on TC adsorption

The effect of initial concentration of TC and contact time on the adsorption capacity of TC are shown in Fig. 9. When the initial TC concentration increased from 50 to 100 mg L^{-1}, the adsorption capacity of the microspheres increased from 13.31 to 19.61 mg g^{-1}. The initial TC concentration was an important factor to influence the adsorption capacity of the microspheres, it is because the higher initial concentration adds contact opportunity of TC and the microspheres, enhance adsorption speed and capacity. Other experiments in this paper were carried out at the initial TC concentration of 100 mg L^{-1}.

As can be clearly seen from Fig. 9, the adsorption capacity of the microspheres increased rapidly with the increase of contact time from 0 to 10 min and more than 70% of equilibrium adsorption capacity for TC occurred within 20 min. After 80 min, the adsorption

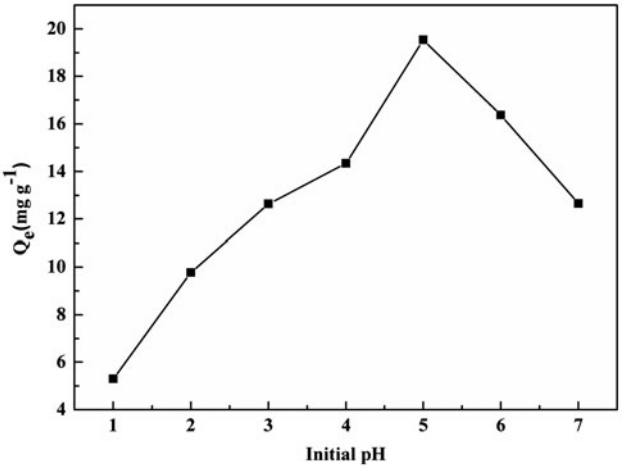

Fig. 8. Effect of initial pH on TCs adsorption (*V*: 20 mL; initial concentration: 100 mg L^{-1}; temperature: 298 K; absorbent dose: 20.0 mg).

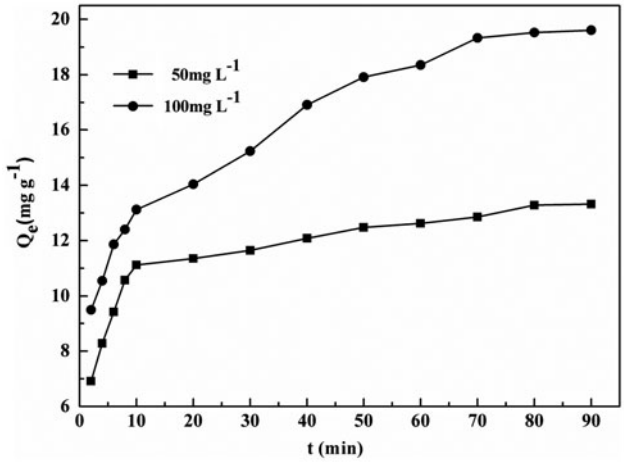

Fig. 9. Effect of initial concentration of TCs and contact time on TCs adsorption (*V*: 20 mL; pH: 5.0; temperature: 298 K; absorbent dose: 20.0 mg).

capacity become constant and the adsorption reached equilibrium. In the initial 10 min, the adsorption capacity of the microspheres increased rapidly was attributed to availability of more adsorption sites. After 10 min, available adsorption sites gradually decreased, adsorption speed of the microspheres became slow. Therefore, for other experiments in this study, 80 min was selected as the contact time.

3.6.4. Effect of temperature on TC adsorption

To study the effect of temperature on the TC adsorption, experiments were conducted by varying adsorption temperature (298, 303, and 308 K). As can be clearly seen from Fig. 10, the equilibrium adsorption capacity of the microspheres increased with the rise of temperature from 298 to 308 K, the adsorption capacity of the microspheres were 21.90, 23.60, and 26.76 mg g^{-1}, respectively, indicated that the adsorption of microspheres was favored at higher temperature and it was controlled by an endothermic process. Based on the above results, it implied that chemical adsorption mechanism may play a vital role in this system [32].

3.6.5. Adsorption kinetic studies

In order to analyze the controlling mechanism of adsorption process of the CTS/HNT-Fe_3O_4 microspheres for TC, the pseudo-first-rate equation and the pseudo-second-rate equation are cited to evaluate the experimental data obtained from batch TC removal experiments [44].

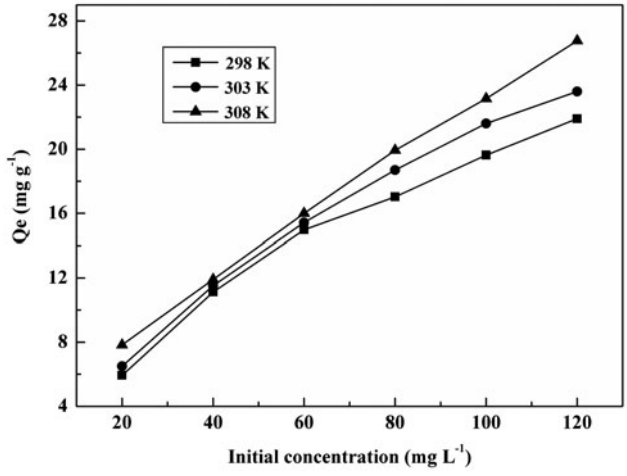

Fig. 10. Effect of temperature on TCs adsorption (V: 20 mL; initial concentration: 100 mg L^{-1}; pH 5.0; absorbent dose: 20.0 mg).

$$\ln(Q_e - Q_t) = \ln Q_e - k_1 t \quad (3)$$

$$\frac{t}{Q_t} = \frac{1}{K_2 Q_e^2} + \frac{t}{Q_e} \quad (4)$$

where Q_e (mg g^{-1}) and Q_t (mg g^{-1}) are the amounts of TC adsorbed on the adsorbent at equilibrium and time t, respectively, k_1 (min^{-1}) is the rate constant of pseudo-first-order kinetic equation, which was calculated from the plot of ln (Q_e–Q_t) vs. t, and k_2 (g mg^{-1} min^{-1}) is the rate constant of pseudo-second-order kinetic equation, which could be obtained from the plot of t/Q_t vs. t.

On the basis of the second-order model, the initial adsorption rate (h, mg g^{-1} min^{-1}) and half-equilibrium time ($t_{1/2}$, min) are summarized in Table 1 and can be represented by Xu et al. [45].

$$h = K_2 Q_e^2 \quad (5)$$

$$t_{1/2} = \frac{1}{K_2 Q_e} \quad (6)$$

The adsorption rate constants and linear regression values of the two rate equations are summarized in Table 1. Fig. 11 displays the fitting curves of the microspheres by pseudo-first-order and the pseudo-second-order kinetic equation. It can be observed that the pseudo-first-order model exhibited poor fitting with low regression coefficients value (R^2) and variance between the experimental and theoretical values. The results indicated that the pseudo-first-order kinetic model was not suitable to describe the adsorption process, while the pseudo-second-order model exhibited favorable fitting between experimental and calculated values of Q_e (with $R^2 > 0.99$), which was assumed that the adsorption of TC followed pseudo-second-order kinetics and chemical process could be the rate-limiting step in the adsorption process for TC [46].

3.6.6. Adsorption isotherm study

The binding properties of the CTS/HNT-Fe_3O_4 microspheres for TC were studied by the equilibrium adsorption experiments. And, the equilibrium data fitting to the Langmuir and Freundlich isotherm models are shown in Fig. 12. The Langmuir isotherm presupposes that the adsorption behavior is based on monolayer adsorption, and the assumption of a structurally homogeneous adsorbent where all sorption sites are

Table 1
Kinetic constants for the pseudo-first-order equation and pseudo-second-order equation

			Pseudo-first-order equation			Pseudo-second-order equation				
T (K)	C_0 (mg/L)	$Q_{e,exp}$ (mg/g)	$Q_{e,c}$ (mg/g)	$k1$ (L min)	R^2	$Q_{e,c}$ (mg/g)	$k2$ (g/mg min)	R^2	h (mg/g min)	$t_{1/2}$ (min)
298	100	19.98	11.21	0.0035	0.97	20.00	0.0094	0.99	3.76	5.32

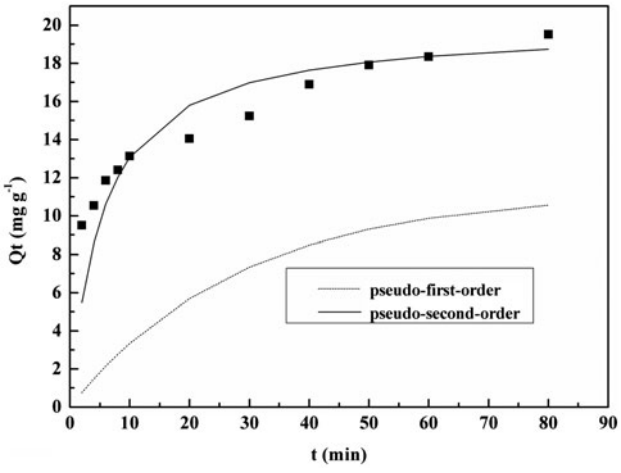

Fig. 11. The adsorption kinetic models of TCs onto the CTS/HNTs-Fe_3O_4 microspheres.

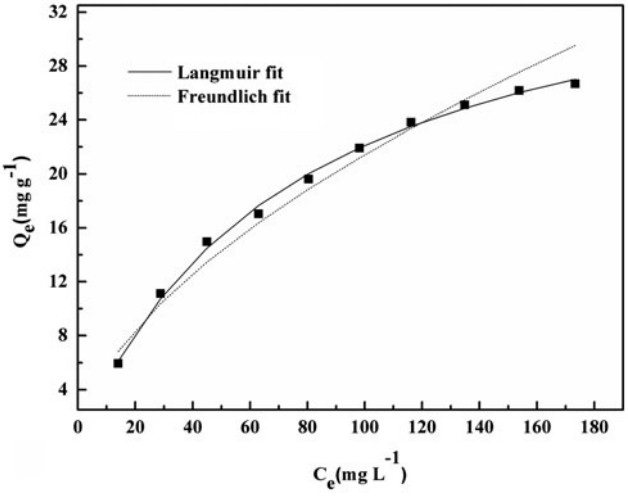

Fig. 12. The adsorption isotherms of TCs onto the CTS/HNTs-Fe_3O_4 microspheres.

identical and energetically equivalent. The Freundlich isotherm was an empirical equation which assumed a heterogeneous surface energy [47]. The nonlinear form of the Langmuir and Freundlich isotherm models were expressed by the following equations, respectively [48].

$$Q_e = \frac{K_L Q_m C_e}{1 + K_L C_e} \tag{7}$$

$$Q_e = K_F C_e^{\frac{1}{n}} \tag{8}$$

where Q_e (mg g^{-1}) is the equilibrium adsorption capacity, C_e (mg L^{-1}) is equilibrium concentration of adsorbate at equilibrium, and Q_m (mg g^{-1}) is the maximum adsorption capacity of the adsorbent. K_L (L mg^{-1}) is the Langmuir adsorption constant, K_F (mg g^{-1}) and n are the Freundlich adsorption equilibrium constants.

The affinity between adsorbate and adsorbent can be predicted using the Langmuir parameter K_L from the dimensionless separation factor R_L,

$$R_L = \frac{1}{1 + C_0 K_L} \tag{9}$$

where C_0 is the initial TC concentration, and K_L is the Langmuir isotherm constant. The adsorption process as a function of R_L may be described as follows: when R_L is greater than one, then, the adsorption reaction is unfavorable, and it is linear, when R_L is equal to one. When R_L is between zero and one, the reaction is favorable, while the reaction is supposed to be irreversible, when R_L is equal to zero. All the calculated values of the adsorption experiment are listed in Table 2.

As can be seen from Fig. 12, the adsorption capacity increased with the increasing concentration of TC, and the maximum adsorption capacity was 26.68 mg g^{-1} at 298 K for the CTS/HNT-Fe_3O_4 microspheres. It can be seen that the linear coefficients of determination (R^2) for the Freundlich isotherm model were lower than R^2 values for the Langmuir isotherm model in Table 2, the Q_m values for the adsorption of TC calculated from the Langmuir model were in close proximity to the experimental data. Obviously, the Langmuir model was much better to describe the adsorption of TC onto the CTS/HNT-Fe_3O_4 microspheres than the Freundlich

Table 2
Adsorption isotherm constants for TCs adsorption onto CTS/HNT-Fe_3O_4 microspheres at 298 K

	Langmuir				Freundlich		
Adsorbent	Q_m (mg g^{-1})	K_L (L mg^{-1})	R_L	R^2	K_F (mg g^{-1})	$1/n$	R^2
CTS/HNT-Fe_3O_4	38.76	0.0133	0.294–0.789	0.996	1.464	0.5827	0.9735

model indicating the surface of the microspheres was homogeneous and a monolayer of TC covered the surface after adsorption [49].

3.6.7. Desorption studies

When considering the cost of the adsorbent, it was necessary to consider the efficiency as well as the preservation of adsorption capacity of the microspheres. In order to evaluate the efficiency and the preservation of adsorption capacity of the microspheres, the consecutive adsorption–desorption process was performed for three times. The concentration of 0.01 M of NaOH solution was used as the desorption agent. Fig. 13 shows the relationship between the time for reuse and the desorption efficiency of CTS/HNT-Fe_3O_4 microspheres for TC. It can be seen that the desorption efficiency of microspheres for TC are 95.41, 92.35, and 90.48%, after the consecutive three-time adsorption–desorption processes. This indicated that CTS/HNT-Fe_3O_4 microspheres had a good reusability in the practical application.

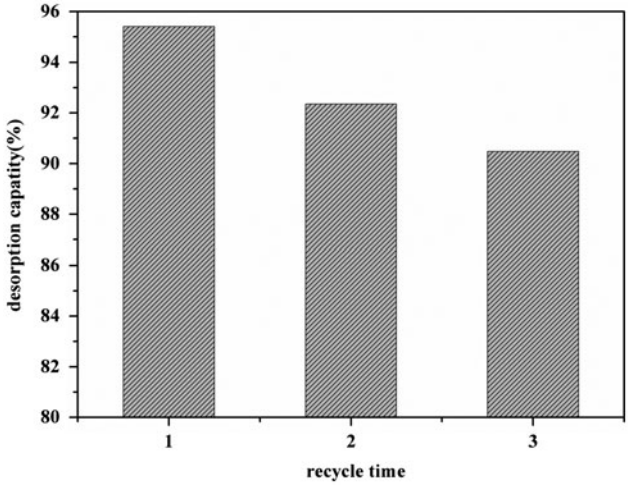

Fig. 13. Desorption and regeneration data (using 0.01 M NaOH).

4. Conclusions

A magnetically separable adsorbent, named CTS/HNT-Fe_3O_4 microspheres was prepared by emulsion cross-linking method. The microspheres were applied as adsorbents for the removal of TC from aqueous solution. The adsorption capacity of CTS/HNT-Fe_3O_4 microspheres increased with an increase in the initial concentration, adsorption temperature, and adsorbent dose. The optimum pH value for TC adsorption is at pH 5.0. The adsorption kinetics was better described by the pseudo-second-order equation, and their adsorption isotherms were better fitted to the Langmuir equation. The reusability of CTS/HNT-Fe_3O_4 microspheres showed no obvious deterioration at least three repeated cycles in performance. The microspheres had the good adsorption capacity and regeneration property and could be easily and rapidly separated from solution phase with the aid of magnetic force and, which could be possibly applied in wastewater removal, biological molecule separation, and drug extraction.

Acknowledgements

This work was financially supported by the National Natural Science Foundation of China (Nos. 21107037 and 21176107), Natural Science Foundation of Jiangsu Province (Nos. BK2011461, BK2011514, and BK2011459), National Postdoctoral Science Foundation (No. 2013M530240), Postdoctoral Science Foundation funded Project of Jiangsu Province (No. 1202002B), and Programs of Senior Talent Foundation of Jiangsu University (No. 12JDG090).

References

[1] H. Liu, Y. Yang, J. Kang, M. Fan, J. Qu, Removal of tetracycline from water by Fe–Mn binary oxide, J. Environ. Sci. 24 (2012) 242–247.
[2] M. Erşan, E. Bağda, E. Bağda, Investigation of kinetic and thermodynamic characteristics of removal of tetracycline with sponge like, tannin based cryogels, Colloids Surf. B: Biointerf. 104 (2013) 75–82.
[3] X. Liu, P. Lv, G. Yao, P. Huo, Y. Yan, Microwave-assisted synthesis of selective degradation photocatalyst

by surface molecular imprinting method for the degradation of tetracycline onto Cl-TiO_2, Chem. Eng. J. 217 (2013) 398–406.
[4] L. Ji, Y. Wan, S. Zheng, D. Zhu, Adsorption of tetracycline and sulfamethoxazole on crop residue-derived ashes: Implication for the relative importance of black carbon to soil sorption, Environ. Sci. Technol. 45 (2011) 5580–5586.
[5] N. Pastor-Navarro, A. Maquieira, R. Puchades, Review on immuno analytical determination of tetracycline and sulfonamide residues in edible products, Anal. Bioanal. Chem. 395 (2009) 907–920.
[6] J. Dai, J. Pan, L. Xu, X. Li, Z. Zhou, R. Zhang, Y. Yan, Preparation of molecularly imprinted nanoparticles with superparamagnetic susceptibility through atom transfer radical emulsion polymerization for the selective recognition of tetracycline from aqueous medium, J. Hazard. Mater. 205 (2012) 179–188.
[7] M.H. Khan, H. Bae, J.Y. Jung, Tetracycline degradation by ozonation in the aqueous phase: Proposed degradation intermediates and pathway, J. Hazard. Mater. 181 (2010) 659–665.
[8] I.R. Bautitz, R.F.P. Nogueira, Degradation of tetracycline by photo-Fenton process-solar irradiation and matrix effects, J. Photochem. Photobiol. A Chem. 187 (2007) 33–39.
[9] J. Bai, Y. Liu, J. Li, B. Zhou, Q. Zheng, W. Cai, A novel thin-layer photoelectrocatalytic (PEC) reactor with double-faced titania nanotube arrays electrode for effective degradation of tetracycline, Appl. Catalysis B Environ. 98 (2010) 154–160.
[10] Y. Liu, X. Gan, B. Zhou, B. Xiong, J. Li, C. Dong, J. Bai, W. Cai, Photoelectrocatalytic degradation of tetracycline by highly effective TiO_2 nanopore arrays electrode, J. Hazard. Mater. 171 (2009) 678–683.
[11] P.H. Chang, Z. Li, T.L. Yu, S. Munkhbayer, Sorptive removal of tetracycline from water by palygorskite, J. Hazard. Mater. 165 (2009) 148–155.
[12] R.A. Figueroa, A. Leonard, A.A. MacKay, Modeling tetracycline antibiotic sorption to clays, Environ. Sci. Technol. 3838 (2004) 476–483.
[13] L. Ji, W. Chen, L. Duan, D. Zhu, Mechanisms for strong adsorption of tetracycline to carbon nanotubes: A comparative study using activated carbon and graphite as adsorbents, Environ. Sci. Technol. 43 (2009) 2322–2327.
[14] P. Kulshrestha, R.F. Giese, D.S. Aga, Investigating the molecular interactions of oxytetracycline in clay and organic matter: Insights on factors affecting its mobility in soil, Environ. Sci. Technol. 38 (2004) 4097–4105.
[15] Y.J. Wang, D.A. Jia, R.J. Sun, H.W. Zhu, D.M. Zhou, Adsorption and cosorption of tetracycline and copper (II) on montmorillonite as affected by solution pH, Environ. Sci. Technol. 42 (2008) 3254–3259.
[16] Z. Xu, J. Fan, S. Zheng, F. Ma, D. Yin, On the adsorption of tetracycline by calcined magnesium–aluminum hydrotalcites, J. Environ. Qual. 38 (2009) 1302–1310.
[17] H. Hou, R. Zhou, P. Wu, L. Wu, Removal of Congo red dye from aqueous solution with hydroxyapatite/chitosan composite, Chem. Eng. J. 211 (2012) 336–342.
[18] R.S. Juang, F.C. Wu, R.L. Tseng, Adsorption removal of copper (II) using chitosan from simulated rinse solutions containing chelating agents, Water Res. 33 (1999) 2403–2409.
[19] W.W. Ngah, L. Teong, M. Hanafiah, Adsorption of dyes and heavy metal ions by chitosan composites: A review, Carbohydr. Polym. 83 (2011) 1446–1456.
[20] L. Wang, A. Wang, Adsorption behaviors of Congo red on the Ns-O-carboxymethyl-chitosan/montmorillonite nanocomposite, Chem. Eng. J. 143 (2008) 43–50.
[21] J. Knaul, M. Hooper, C. Chanyi, K.A. Creber, Improvements in the drying process for wet-spun chitosan fibers, J. Appl. Polym. Sci. 69 (1998) 1435–1444.
[22] A. Ramesh, H. Hasegawa, W. Sugimoto, T. Maki, K. Ueda, Adsorption of gold (III), platinum (IV) and palladium (II) onto glycine modified crosslinked chitosan resin, Bioresour. Technol. 99 (2008) 3801–3809.
[23] W.S.W. Ngah, L.C. Teong, M. Hanafiah, Adsorption of dyes and heavy metal ions by chitosan composites: A review, Carbohydr. Polym. 83 (2011) 1446–1456.
[24] D.G. Shchukin, G.B. Sukhorukov, R.R. Price, Y.M. Lvov, Halloysite nanotubes as biomimetic nanoreactors, Small 1 (2005) 510–513.
[25] W. Jinhua, Z. Xiang, Z. Bing, Z. Yafei, Z. Rui, L. Jindun, C. Rongfeng, Rapid adsorption of Cr(VI) on modified halloysite nanotubes, Desalination 259 (2010) 22–28.
[26] M.H. Shamsi, K.E. Geckeler, The first biopolymer-wrapped non-carbon nanotubes, Nanotechnology 19 (2008) 075604.
[27] G. Cavallaro, G. Lazzara, S. Milioto, Modified halloysite nanotubes: Nanoarchitectures for enhancing the capture of oils from vapor and liquid phases, ACS Appl. Mater. Interface 2013 (2013) 606–612.
[28] G. Cavallaro, A. Gianguzza, G. Lazzara, Alginate gel beads filled with halloysite nanotubes, Appl. Clay Sci. 72 (2013) 132–137.
[29] Y. Ye, H. Chen, J. Wu, Evaluation on the thermal and mechanical properties of HNT-toughened epoxy/carbon fibre composites, Compos. Part B: Eng. 42 (2011) 2145–2150.
[30] S. Hsu, P.C. Singer, Removal of bromide and natural organic matter by anion exchange, Water Res. 44 (2010) 2133–2140.
[31] T.H. Boyer, P.C. Singer, Stoichiometry of removal of natural organic matter by ion exchange, Environ. Sci. Technol. 42 (2007) 608–613.
[32] D. Chen, W. Li, Y. Wu, Q. Zhu, Z. Lu, G. Du, Preparation and characterization of chitosan/montmorillonite magnetic microspheres and its application for the removal of Cr(VI), Chem. Eng. J. 221 (2013) 8–15.
[33] J.L. Gong, B. Wang, G.M. Zeng, C.P. Yang, C.G. Niu, Q.Y. Niu, W.J. Zhou, Y. Liang, Removal of cationic dyes from aqueous solution using magnetic multi-wall carbon nanotube nanocomposite as adsorbent, J. Hazard. Mater. 164 (2009) 1517–1522.
[34] P. Liu, Z. Su, Attapulgite-Fe_3O_4 magnetic nanoparticles via co-precipitation technique, Appl. Surf. Sci. 255 (2008) 2020–2025.
[35] Y. Xie, D. Qian, D. Wu, Magnetic halloysite nanotubes/iron oxide composites for the adsorption of dyes, Chem. Eng. J. 168 (2011) 959–963.
[36] P. Luo, Y. Zhao, B. Zhang, J. Liu, Y. Yang, J. Liu, Study on the adsorption of neutral red from aqueous solution onto halloysite nanotubes, Water Res. 44 (2010) 1489–1497.

[37] E. Tierrablanca, J. Romero-García, P. Roman, R. Cruz-Silva, Biomimetic polymerization of aniline using hematin supported on halloysite nanotubes, Appl. Catal. A: Gen. 381 (2010) 267–273.
[38] P.R. Chang, J. Yu, X. Ma, D.P. Anderson, Polysaccharides as stabilizers for the synthesis of magnetic nanoparticles, Carbohydr. Polym. 83 (2011) 640–644.
[39] A. Pawlak, M. Mucha, Thermogravimetric and FTIR studies of chitosan blends, Thermochim. Acta 396 (2003) 153–166.
[40] W. Tan, Y. Zhang, Y.S. Szeto, L. Liao, A novel method to prepare chitosan/montmorillonite nanocomposites in the presence of hydroxy-aluminum oligomeric cations, Compos. Sci. Technol. 68 (2008) 2917–2921.
[41] M. Liu, Y. Zhang, C. Wu, S. Xiong, C. Zhou, Chitosan/halloysite nanotubes bionanocomposites: Structure, mechanical properties and biocompatibility, Int. J. Biol. Macromol. 51 (2013) 566–575.
[42] Z. Liu, F.S. Zhang, R. Sasai, Arsenate removal from water using Fe_3O_4-loaded activated carbon prepared from waste biomass, Chem. Eng. J. 160 (2010) 57–62.
[43] Q. Yu, S. Deng, G. Yu, Selective removal of perfluorooctane sulfonate from aqueous solution using chitosan-based molecularly imprinted polymer adsorbents, Water Res. 42 (2008) 3089–3097.
[44] D. Mulange wa Mulange, A.M. Garbers-Craig, Stabilization of Cr(VI) from fine ferrochrome dust using exfoliated vermiculite, J. Hazard. Mater. 223 (2012) 46–52.
[45] L. Xu, J. Dai, J. Pan, X. Li, P. Huo, Y. Yan, X. Zou, R. Zhang, Performance of rattle-type magnetic mesoporous silica spheres in the adsorption of single and binary antibiotics, Chem. Eng. J. 174 (2011) 221–230.
[46] G. Baydemir, M. Andaç, N. Bereli, R. Say, A. Denizli, Selective removal of bilirubin from human plasma with bilirubin–imprinted particles, Indust. Eng. Chem. Res. 46 (2007) 2843–2852.
[47] X. Wang, J. Pan, W. Guan, J. Dai, X. Zou, Y. Yan, C. Li, W. Hu, Selective removal of 3-chlorophenol from aqueous solution using surface molecularly imprinted microspheres, J. Chem. Eng. Data 56 (2011) 2793–2801.
[48] J. Pan, X. Zou, X. Wang, W. Guan, Y. Yan, J. Han, Selective recognition of 2,4-dichlorophenol from aqueous solution by uniformly sized molecularly imprinted microspheres with β-cyclodextrin/attapulgite composites as support, Chem. Eng. J. 162 (2010) 910–918.
[49] P. Luo, Y.F. Zhao, B. Zhang, J.D. Liu, Study on the adsorption of neutral red from aqueous solution onto halloysite nanotubes, Water Res. 44 (2010) 1489–1497.